Peculiar radio-X-ray relationship in active stars

Vedantham, H.K.; Callingham, J.R.; Shimwell, T.W.; Benz, A.O.; Hajduk, M.; Ray, T.P.; ... ; Drabent, A.

The Astrophysical Journal Letters, 926:L30 (8pp), 2022 February 20 https://doi.org/10.3847/2041-8213/ac5115

Peculiar Radio–X-Ray Relationship in Active Stars

H. K. Vedantham[1,2], J. R. Callingham[1,3], T. W. Shimwell[1,3], A. O. Benz[4], M. Hajduk[5,6], T. P. Ray[7], C. Tasse[8,9], and A. Drabent[10]
[1] ASTRON, Netherlands Institute for Radio Astronomy, Oude Hoogeveensedijk 4, Dwingeloo, 7991 PD, The Netherlands; vedantham@astron.nl
[2] Kapteyn Astronomical Institute, University of Groningen, P.O. Box 72, 97200 AB, Groningen, The Netherlands
[3] Leiden Observatory, Leiden University, P.O. Box 9513, 2300 RA Leiden, The Netherlands
[4] Institute for Particle Physics and Astrophysics, ETH Zurich, 8093 Zürich, Switzerland
[5] Space Radio-Diagnostics Research Centre, University of Warmia and Mazury, ul.Oczapowskiego 2, 10-719 Olsztyn, Poland
[6] Department of Astrophysics/IMAPP, Radboud University, P.O. Box 9010, 6500 GL Nijmegen, The Netherlands
[7] School of Cosmic Physics, Dublin Institute for Advanced Studies, 31 Fitzwilliam Place, Dublin, D02 XF86, Ireland
[8] GEPI & USN, Observatoire de Paris, Université PSL, CNRS, 5 Place Jules Janssen, F-92190 Meudon, France
[9] Department of Physics & Electronics, Rhodes University, P.O. Box 94, Grahamstown, 6140, South Africa
[10] Thüringer Landessternwarte, Sternwarte 5, D-07778 Tautenburg, Germany
Received 2021 December 8; revised 2022 February 1; accepted 2022 February 2; published 2022 February 22

Abstract

The empirical relationship between the nonthermal 5 GHz radio luminosity and the soft X-ray luminosity of active stellar coronae, canonically called the Güdel–Benz relationship, has been a cornerstone of stellar radio astronomy, as it explicitly ties the radio emission to the coronal heating mechanisms. The relationship extends from microflares on the Sun to the coronae of the most active stars suggesting that active coronae are heated by a flare-like process. The relationship is thought to originate from a consistent partition of the available flare energy into relativistic charges, which emit in the radio-band via the *incoherent* gyrosynchrotron mechanism, and heating of the bulk coronal plasma, which emits in the X-ray band via the Bremsstrahlung mechanism. Consequently, *coherent* emission from stellar and substellar objects is not expected to adhere to this empirical relationship, as it is observed in ultracool dwarf stars and brown dwarfs. Here we report a population of radio-detected chromospherically active stars that surprisingly follow the Güdel–Benz relationship despite their radio emission being classified as coherent emission by virtue of its high circularly polarized fraction and high brightness temperature. Our results prompt a reexamination of the physics behind the Güdel–Benz relationship, its implication for the mechanism of coronal heating and particle acceleration in active stars, and the phenomenological connection between solar and stellar flares.

Unified Astronomy Thesaurus concepts: Stellar coronae (305)

1. Introduction

There exists an empirical quasi-linear relationship, called the Güdel–Benz relationship, between the X-ray luminosity (L_X [erg s^{-1}]) and the quasi-quiescent, nonthermal 5 GHz radio spectral luminosity (L_R [erg s^{-1} Hz^{-1}]) in chromospherically active stars and binaries: $L_X \approx L_R \times 10^{15.5}$ (Drake et al. 1989; Güdel & Benz 1993; Benz & Güdel 1994). The relationship holds for soft X-ray luminosities ranging from $\sim 10^{29}$ to 10^{32} erg s^{-1} and the corresponding radio immensities ranging from 10^{22} to 10^{28} erg s^{-1}. The soft X-ray emission is due to thermal Bremsstrahlung in the coronal plasma, whereas the radio emission is thought to be due to incoherent gyrosynchrotron emission from relativistic electrons gyrating in the coronal magnetic field. The relationship also extends all the way down the energy-scale to microflares from the Sun that have $L_X \sim 10^{25}$ erg s^{-1} (Benz & Güdel 1994), suggesting a common flare-like mechanism that deposits energy into the coronae of the Sun and active stars alike.

The Güdel–Benz relationship is canonically explained in one of two ways, both of which require a consistent fraction of energy in flares to go to accelerating charges to relativistic speeds (Güdel & Benz 1993; Benz & Güdel 1994, 2010). One way posits that all of the flare energy goes to relativistic charges. These charges lose a tiny fraction of their energy to gyrosynchrotron emission while the bulk of their energy eventually heats up the corona that emits the thermal X-ray emission. The second way is that a small, albeit consistent, fraction of the flare energy goes into relativistic particles while the remainder directly heats the ambient coronal gas. It is also plausible that a different phenomenon (e.g., electric currents or Alfvén waves (Mandrini et al. 2000) drives the coronal heating and particle acceleration, but the consistent energy partitioning remains necessary to explain the relationship.

Although the coronal heating mechanism is not fully understood, the above explanations are generally accepted (Güdel 2002) at a qualitative level. However, at the macro level, the relationship forces a linkage between physical parameters such as the coronal magnetic field strength, the cooling timescale of relativistic charges, the fraction of flare energy that goes into relativistic charges, and the X-ray luminosity (Güdel & Benz 1993). These parameters are not readily accessible by independent measurements, which has led to a longstanding debate as to the precise microphysics of the relationship, its implications for the coronal heating problem, and whether the Sun and active stars share a common flare-like coronal phenomenon (Holman 1986; Airapetian & Holman 1998; Forbrich et al. 2011).

More recently, several detections of mildly circularly polarized quasi-quiescent emission were made in ultracool dwarf stars and brown dwarfs. When plotted against the Güdel–Benz relationship,

these objects consistently proved radio-loud or X-ray-dim (Berger et al. 2001; Berger 2002; McLean et al. 2012; Williams et al. 2014). One explanation offered for the breakdown of the Güdel–Benz relationship in the ultracool dwarf regime is that the radio emission is not due to the gyrosynchrotron mechanism but due to the coherent cyclotron maser mechanism that appears only mildly polarized because of depolarization during propagation in the magnetosphere (Hallinan et al. 2008). An alternate explanation posits that the quasi-quiescent radio emission is gyrosynchrotron, but the energetics of these systems or their magnetospheric structure do not support a stable thermal corona to form, which leads to their X-ray under-luminosity (Berger et al. 2010; Williams et al. 2014). More recently, Leto et al. (2021) have argued that the electron acceleration mechanism in dipole-dominated objects (from magnetic A/B stars to gas giant planets) is fundamentally different from the flare acceleration seen in the Sun and active stars and that this difference leads to a breakdown of the radio–X-ray relationship in such objects, even though the mildly polarized radio emission may be gyrosynchrotron in origin.

Regardless of the above debate on *mildly* polarized emission in ultracool dwarfs, it is widely accepted that *highly* polarized radio emission (several tens of per cent) is the result of a coherent emission mechanism and therefore must not adhere to the Güdel–Benz relationship. This claim is based on the fact that, unlike incoherent gyrosynchrotron emission, coherent emission mechanisms in stellar coronae (and planetary magnetosphere) are ultimately driven by plasma instabilities that are sensitive to the *gradient* in the electron momentum distribution[11] and not to the total energy of the emitting electrons. Additionally, the efficiency of radio emission for incoherent gyrosynchrotron and coherent mechanisms is vastly different. The two mechanisms are therefore not expected to adhere to the same scaling law with coronal X-ray luminosities. Indeed, this is the case for highly polarized radio emission at 144 MHz from M dwarfs—they do not follow the Güdel–Benz relationship, nor establish a new scaling law (Callingham et al. 2021b).

Here we report that highly polarized emission from RS Cvn binaries and other high-activity stars at 144 MHz unexpectedly follows the Güdel–Benz relationship, upending decades-long and widely accepted heuristics commonplace in stellar radio astronomy analysis. Our results prompt a reexamination of the physics behind the Güdel–Benz relationship and of the mechanism of radio emission from active stars. We outline a few plausible unified models that can reconcile the historical data with our data and motivate future radio observations that can test these models.

The rest of the paper is organized as follows. Section 2 is devoted to describing the data and ruling out statistical biases as the cause of the anomalous adherence to the Güdel–Benz relationship in our sample. In Section 3, we discuss possible resolutions to this anomalous result and end with the concluding remarks and outlook in Section 4.

2. Data and Statistical Tests

We are presently conducting a systematic survey of the northern sky for stellar, brown dwarf, and exoplanetary radio emissions (see, e.g., Vedantham et al. 2020a, 2020b; Callingham et al. 2021a, 2021b; Davis et al. 2021). We primarily identify our targets in the pipeline-processed data from the Low-frequency Array (LOFAR) Two-meter Sky Survey (LoTSS; Shimwell et al. 2017, 2019; Tasse et al. 2021) as circularly polarized sources in the Stokes *V* component of the survey (V-LoTSS; Callingham et al. 2022, in preparation). Of these, we have previously presented 14 active binaries (Toet et al. 2021). Here, we report six additional chromospherically active stars also discovered as highly circularly polarized radio sources in LoTSS. These stars have circular fractions between ≈50% and 90%. Since stars close to our Stokes *I* detection threshold will not pass the threshold in Stokes *V*, we separately searched for Stokes *I* emission from astrometrically associated stars in the catalog of chromospherically active binaries compiled by Eker et al. (2008). This yielded four additional RS CVn detections all between 0.6 and 0.8 mJy. Because the typical noise rms values in the LoTSS images are between 70 and 100 μJy, any polarization fraction in these sources of about 60% or lower would not have crossed the detection threshold of our Stokes *V*–only search (J. R. Callingham et al. 2022, in preparation). We include these stars for completeness, although excluding them from our analysis does not change the results and argument presented here. All of our detections are summarized in Table 1.

The X-ray flux densities for our active sources were determined by identifying their counterparts in the Second ROSAT all-sky survey (2RXS) source catalog (Boller et al. 2016). We considered an association as reliable when the proper-motion-corrected Gaia Data Release 2 (DR2; Gaia Collaboration et al. 2018) position of radio-bright active binaries was within 1′ of a 2RXS source position. All of our sources are detected in 2RXS, as opposed to the serendipitous survey catalogs produced by XMM Newton or Chandra, providing us with a homogeneous X-ray data set. Furthermore, as the original Güdel–Benz relationship was established with ROSAT data (Benz & Güdel 1994), we do not need to scale or adjust the X-ray data for different wavelength coverage.

The reported 2RXS count rates for our radio detected active stars are listed in Table 1. The count rate was converted to a 0.1–2.4 keV flux via the conversion factor $\mathrm{CF} = (5.30\mathrm{HR1} + 8.31) \times 10^{-12}$ erg cm^{-2} count^{-1}, where HR1 is the hardness ratio in the soft ROSAT band (Fleming et al. 1995). We note that it is likely that ≈20% of our detections were observed during an X-ray flaring event considering the brevity of the ROSAT observations (Pandey & Singh 2012). Such variable X-ray activity does not preclude investigating the Güdel–Benz relationship as an X-ray flare from an RS CVn binary rarely more than doubles its X-ray flux (Pandey & Singh 2012). The X-ray variability of active binaries will produce scatter within the Güdel–Benz relationship, as already observed for the canonical Güdel–Benz data set (Benz & Güdel 1994) with its ∼0.6 dex scatter around the best fit (Williams et al. 2014).

Figure 1 shows our sample in the radio–X-ray luminosity plane along with the canonical Güdel–Benz relationship and the archival sample that led to the discovery of the relationship (Güdel & Benz 1993; Benz & Güdel 1994). The figure shows a remarkable adherence of our sample to the empirical law. A Kendall tau test confirms a monotonic relationship between the radio and X-ray luminosity of our sample with a correlation coefficient of 0.6 and a *p*-value for the null hypothesis of 1.3×10^{-5}.

The bottom panel of Figure 1 shows the scatter of our sample with respect to the Güdel–Benz relationship. We clearly see

[11] Strictly speaking, this is true in the absence of saturation (see also Section 3.4).

Table 1
List of Detected Stars in LoTSS DR2 whose Radio and X-Ray Luminosities are Plotted in Figure 1

Common Name	Type	S_I (mJy)	S_V (mJy)	X-ray lum. (count s^{-1})	Parallax (mas)	Pol. frac (per cent)	X-ray lum (erg s^{-1})
Sig CrB	RS Cvn	7.53 ± 0.28	-5.82 ± 0.18	9.46	47.44	-77 ± 3	4.4
BQ CVn	RS Cvn	2.24 ± 0.22	-1.78 ± 0.15	0.43	5.5982	-79 ± 10	13.5
FG UMa	RS Cvn	0.62 ± 0.16	0.49 ± 0.10	0.37	4.7389	79 ± 26	17.4
BF Lyn	RS Cvn	1.91 ± 0.29	1.46 ± 0.16	3.04	42.6303	76 ± 14	1.7
DM UMa	RS Cvn	3.20 ± 0.26	-1.72 ± 0.16	0.94	5.2803	-53 ± 6	29.3
EV Dra	RS Cvn	3.03 ± 0.28	-2.61 ± 0.20	0.91	17.3764	-86 ± 10	2.8
DG CVn	RS Cvn	0.63 ± 0.11	-0.57 ± 0.06	0.43	54.6875	-90 ± 18	0.1
EZ Peg	RS Cvn	0.87 ± 0.20	0.75 ± 0.09	0.67	6.0817	86 ± 22	19.1
BH CVn	RS Cvn	2.10 ± 0.40	1.11 ± 0.11	2.68	21.6693	52 ± 11	5.5
WW Dra	RS Cvn	0.54 ± 0.13	-0.38 ± 0.08	0.51	6.5160	-70 ± 22	12.7
YY Gem	RS Cvn	1.87 ± 0.26	-0.87 ± 0.09	3.72	66.2323	-46 ± 8	0.8
II Peg	RS Cvn	3.74 ± 0.37	2.61 ± 0.21	10.77	25.4046	69 ± 8	15.1
BD+33 4462	RS Cvn	1.62 ± 0.42	-0.86 ± 0.20	0.2	4.5922	-53 ± 18	13.1
FG Cam	RS Cvn	1.83 ± 0.23	-1.16 ± 0.18	0.46	3.1970	-63 ± 12	63.3
BD+42 2437	Ro Var	0.50 ± 0.13	-0.37 ± 0.09	0.31	4.3684	-74 ± 26	16.5
FK Com	FK Com	3.40 ± 0.31	2.56 ± 0.21	0.21	4.6102	75 ± 9	9.3
OU And	Ro Var	1.51 ± 0.28	1.26 ± 0.24	0.69	7.1692	83 ± 22	19.1
ksi UMa	RS CVn	0.65 ± 0.12	-0.40 ± 0.12	4.92	114.4867	-61 ± 21	0.3
FI Cnc	FK Com	0.83 ± 0.12	0.69 ± 0.08	0.82	10.0082	83 ± 15	9.7
FF UMa	RS Cvn	1.48 ± 0.24	-1.10 ± 0.13	2.20	8.7324	-74 ± 14	28.6
44 Boo	W UMa	1.21 ± 0.31	-0.46 ± 0.12	4.73	79.95	-38 ± 13	0.7
V835 Her	RS Cvn	0.58 ± 0.10		1.89	32.1839		1.8
Sig Gem	RS Cvn	0.72 ± 0.14		8.15	26.08		12.7
IM Peg	RS Cvn	0.85 ± 0.17		2.86	10.0496		30.8

Note. S_I and S_V correspond to the 144 MHz total and circularly polarized flux density, respectively. The X-ray count rate is for the 0.1–2.4 keV band from 2RXS (Boller et al. 2016). The parallax measurements are mostly from Gaia DR2 (Gaia Collaboration et al. 2018). For the brightest systems (e.g., ksi UMa and 44 Boo), the parallax measurements come from the updated Hipparcos catalog (van Leeuwen 2007). The error in the polarized fraction is computed by Taylor expanding the quotient (V/I) to first order and assuming that the Stokes V and Stoker I noise are independent (see Appendix of Vedantham & Koopmans 2016). The horizontal line separates systems with circularly polarized counterparts from systems with only detections in the total intensity, which are located below the line. Source types are taken from Toet et al. (2021, and references therein) and from the Simbad archive server. "Ro Var" implies "rotational variable" as the exact variable class for BD +42 2437 is unknown in the literature. Our Stokes V handedness definition is identical to that used by Callingham et al. (2021b), namely, left-handed minus right-handed.

that our sample adheres to the Güdel–Benz relationship as well as the original 5 GHz sample that was used to establish this empirical relationship.

To ensure that the adherence of our sample to the Güdel–Benz relationship is neither random happenstance nor a statistical artifact of sample incompleteness inherent in flux-limited surveys (radio in our case), we ran a simple Monte Carlo simulation that produces 1000 synthetic radio and X-ray data sets under the null hypothesis (i.e., radio and X-ray flux are independent random variables). We assumed a space density of X-ray detected active stars that are also radio emitters of $n = 10^{-5}\,\mathrm{pc}^{-3}$, a distance horizon of 200 pc, both consistent with our detections in LoTSS, and a lognormal distribution of X-ray and radio luminosity. The two distributions were assumed to be independent (as consistent with the null hypothesis). The simulation horizon was chosen to represent the high Galactic latitude of the fields surveyed so far by our LoTSS data. It also agrees to within a factor of order unity with the farthest radio detection in our population. The space density of radio emitters was chosen such that the mean number of detection in the Monte Carlo runs was equal to the number of detections in our sample. For the radio luminosity distribution, we assumed a mean of $\langle L_{\mathrm{rad}} \rangle = 10^{16}\,\mathrm{erg\,s^{-1}\,Hz^{-1}}$ and standard deviation of $\sigma_{\mathrm{rad}} = 10^{1}\,\mathrm{erg\,s^{-1}\,Hz^{-1}}$, while for the X-ray luminosity we assumed $\langle L_{\mathrm{X}} \rangle = 10^{31}\,\mathrm{erg\,s^{-1}}$ and $\sigma_{\mathrm{X}} = 10^{0.75}\,\mathrm{erg\,s^{-1}}$. These values were chosen to approximately span the range of observed radio and X-ray immensities (see Figure 1).

The top panel of Figure 2 shows the output of a randomly chosen simulation run in the L_{X}, L_R plane, and the bottom panel shows the histogram of the 10^5 Kendall tau rank correlation coefficients from simulations. The simulations reject the null hypothesis with a p-value of $<10^{-4}$. We therefore conclude that our empirical result is not due to chance or a bias due to the volume incompleteness of our radio survey.

All the stars in our sample are highly circularly polarized radio emitters in the meter-wave band (Table 1) with high brightness temperatures, which suggests that the emission mechanism is a coherent one. Toet et al. (2021) showed that, based on the brightness temperature inferred from typical coronal sizes and the emitters' polarized fraction, the emission mechanism is the electron cyclotron maser. On the other hand, the emission mechanism in the centimeter-wave sample that established the Güdel–Benz relationship is the gyrosynchrotron mechanism. The two radio data sets have also been observed at vastly different radio frequencies, and the two emission mechanisms have different emissivities. It is therefore remarkable and puzzling that our sample follows the Güdel–Benz relationship. It implies that either the inference of the emission mechanism in previous works is wrong or there is a deeper physical reason for why the presumed gyrosynchrotron emission at 5 GHz emission and the presumed coherent emission at 144 MHz emission have approximately the same spectral luminosity.

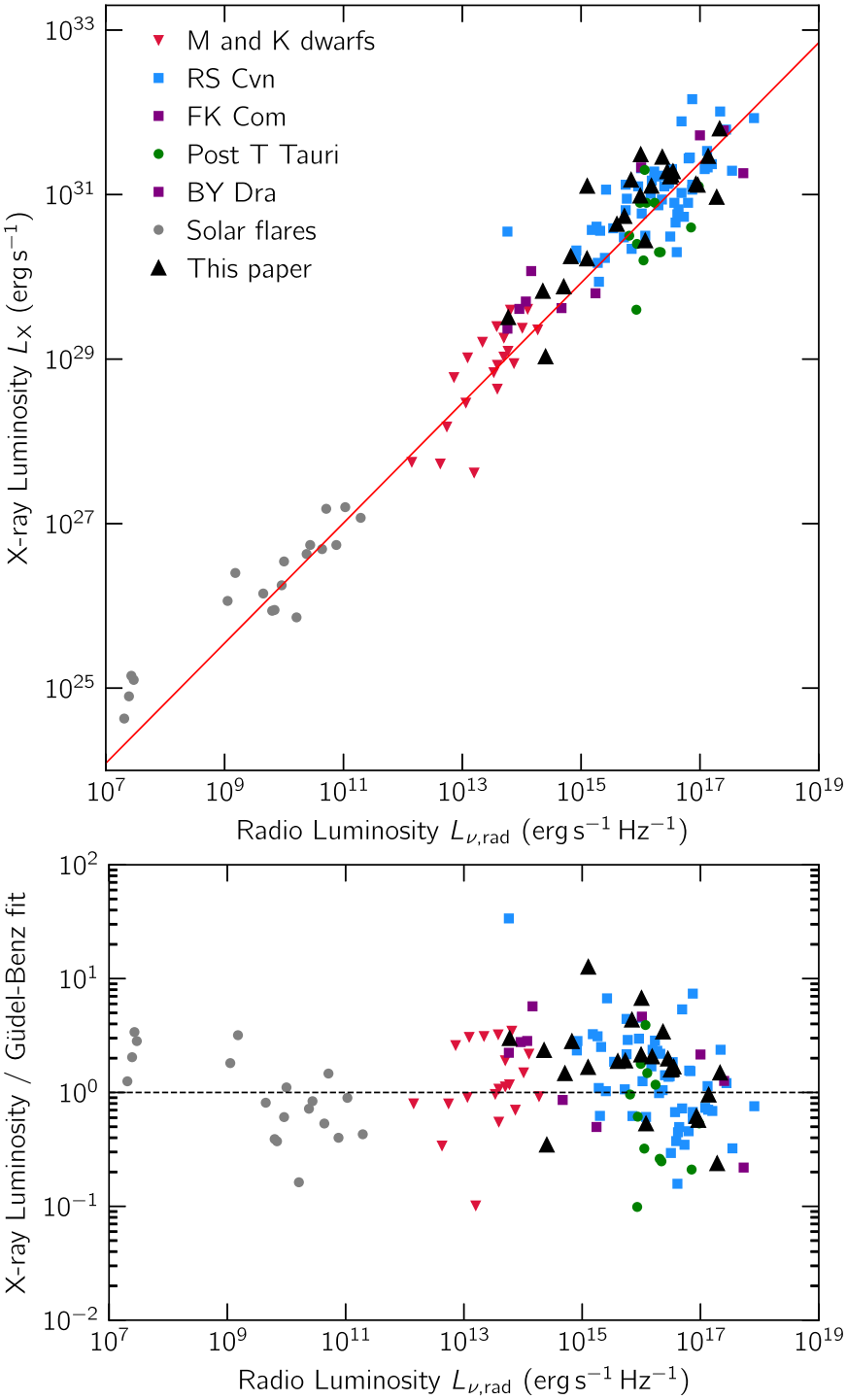

Figure 1. Top panel: The peculiar adherence of our highly polarized sample at 144 MHz (total flux), shown in black triangles, to the Güdel–Benz relationship shown by the solid red line, $L_X = 9.48 \times 10^{18} L_{\nu,\mathrm{rad}}^{0.73}$ (Williams et al. 2014). The other points are literature values at 5 GHz that were initially used to establish the Güdel–Benz relationship (Benz & Güdel 1994). The X-ray flux is in the 0.1–2.4 keV band. Bottom panel: Dispersion of the data from the Güdel–Benz relationship showing that our sample has the same level of scatter as the 5 GHz data from the literature.

3. Discussion

Now that we are faced with an empirically established adherence of highly polarized meter-wave emission to the canonical Güdel–Benz relationship, we turn our attention to seeking an explanation. In doing so, our aim is not to construct a detailed model of the coronal parameters and their spatial structure but rather to argue from first principles and chart out plausible paths to a resolution.

We will first posit that both the centimeter-wave and meter-wave emission must originate from the same emission mechanism and that the mechanism generates a flat spectrum. This is motivated by the fact that the three possible emission mechanisms, which are gyrosynchrotron, plasma, and cyclotron maser, all have remarkably different efficiencies and will require contrived scenarios to achieve the observed flux density parity. With this assumption, we have three choices for the common emission mechanism.

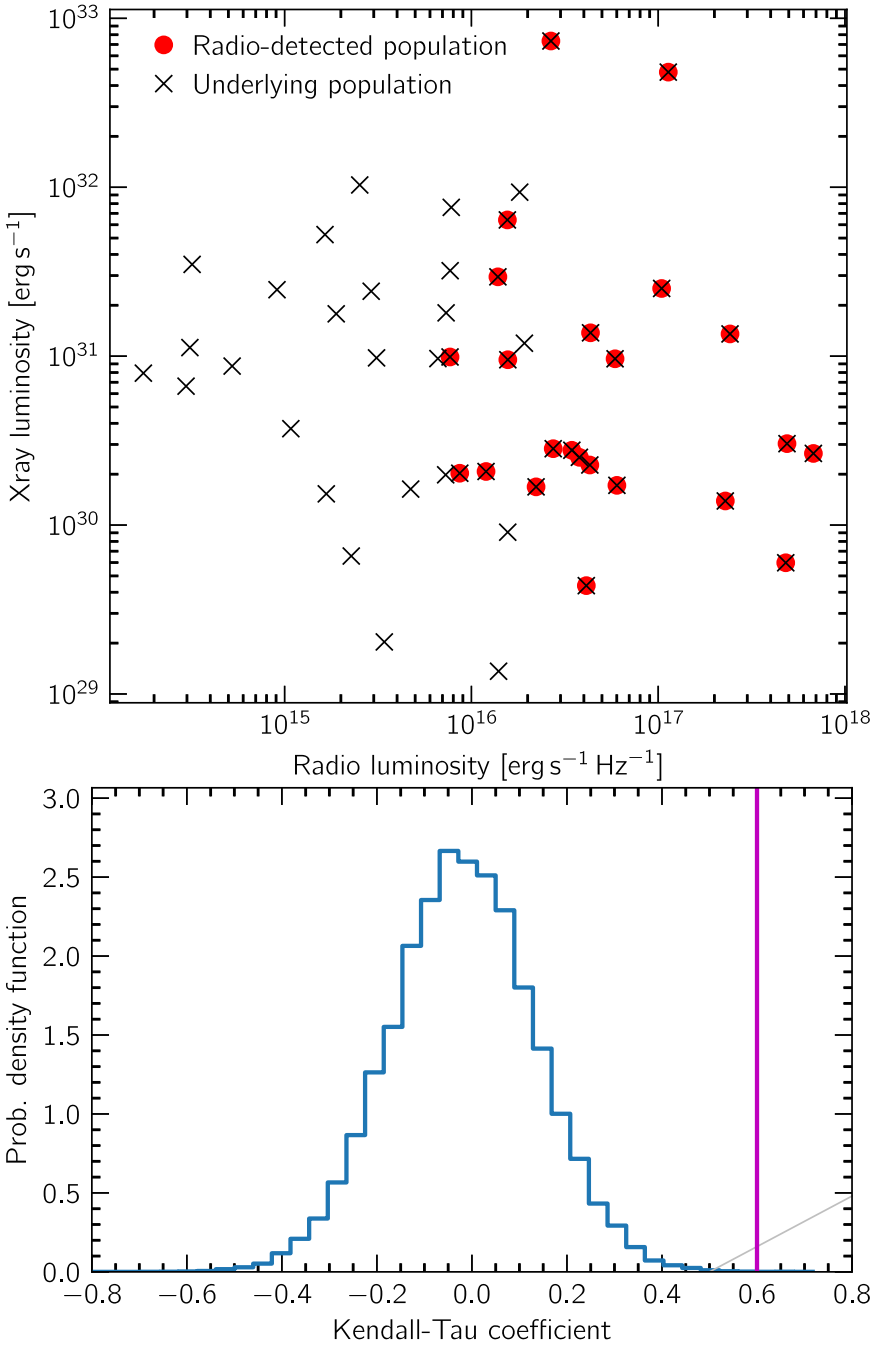

Figure 2. Results of the Monte Carlo simulation of radio and X-ray detections under the null hypothesis (i.e., radio and X-ray luminosities are uncorrelated). The top panel shows the sample (black crosses) and the subset that will cross the radio-detection threshold of our survey (red circles), in one realization. The bottom panel shows the distribution of the Kendall tau correlation coefficient between the radio and X-ray luminosity of the radio-detected population from 10^5 realizations (blue step curve) in comparison to the measured coefficient from our sample (magenta line).

3.1. Gyrosynchrotron

The centimeter-wave observations have previously been widely interpreted as gyrosynchrotron[12] (Benz & Güdel 2010), so we only need to focus our attention on interpreting the meter-wave emission. The main challenges to be addressed here are the high circularly polarized fraction and high brightness temperature at 144 MHz. The polarization fraction of our sample spans from about 40% to 86%, whereas the brightness temperature of our sample, assuming a source to be a disk of radius equal to the photometric stellar radius, spans from $T_b \approx 10^{11.5}$ K to $T_b \approx 10^{13}$ K.

Synchrotron emission is only weakly circularly polarized even when dispersive effects of the underlying thermal medium (i.e., the Razin–Tsytovich effect; Ginzburg & Syrovatskii 1964) are taken into consideration (Melrose 1971b). The only known regimes where synchrotron emission generates levels of circular polarization of $\gtrsim$50% are (a) in the presence of a highly anisotropic pitch-angle distribution of emitting charges

[12] We will use the usual convention and refer to Magnetobremsstrahlung as gyrosynchrotron when emission primarily appears at moderate harmonics between ≈10 to ≈100 and as synchrotron emission in the ultrarelativistic limit.

and (b) emission at low harmonics of the cyclotron frequency by mildly relativistic charges.[13]

3.1.1. Low Pitch-angle Regime

The regime $\gamma \sin\alpha \lesssim 1$, where γ is the characteristic electron Lorentz factor and α is the pitch angle, is appealing for generating the observed 144 MHz properties. This is the "small pitch-angle" regime where the ultrarelativistic approximation commonly made (e.g., chapter 6 of Rybicki & Lightman 1986) breaks down. We refer the reader to O'Dell & Sartori (1970), Melrose (1971a), and Epstein (1973) for a discussion of this regime. In this case, the bulk of the radiation is beamed within a cone oriented along the magnetic field with an opening angle given by $\theta \approx \alpha\gamma^{-1}$ and is highly circularly polarized. The emission in the observer frame is the Doppler-boosted cyclotron frequency, given by $\nu = 2\nu_B\gamma/(1+\gamma^2\theta^2)$ in the ultrarelativistic limit, where ν_B is the nonrelativistic electron cyclotron frequency. The observed emission therefore appears at a frequency of $\sim\gamma\nu_B$ with a fractional bandwidth of order unity. This may be contrasted with the moderate and high pitch-angle regimes from canonical theory, which yields weakly circularly polarized broadband emission centered around a much larger critical frequency of $\gamma^2 \sin\alpha\nu_B$.

With the above theory, a plausible scenario emerges. The electron acceleration process generates relativistic electrons ($\gamma \lesssim 10$) within a narrow forward cone ($\alpha \lesssim 0.1$). These electrons emit in the LOFAR band in the small pitch-angle regime. Their pitch angle distribution eventually broadens due to collision or other processes leading to mildly polarized emission in the centimeter-wave band by the gyrosynchrotron mechanism. Coming to the issue of brightness temperature, regardless of the kinetic temperature of the emitting electrons and their combined optical depth, the brightness temperature cannot exceed the inverse Compton limit of $\approx 10^{12}$ K.[14] Therefore, stars in our sample at the upper end of the brightness temperature limit of $\approx 10^{13}$ K necessarily imply rather large source sizes of at least a few stellar radii. Hence, in this scenario, the emission must come from the bulk of the corona and not the small coronal loops close to the stellar surface. Specific limits on the source size must, however, await detailed radiative transfer modeling for the postulated case of a directed beam of electrons injected into a large-scale magnetic trap (such as a dipolar trap) in the presence of a background dispersive plasma.

3.1.2. Emission at Low Harmonics

In the relativistic limit, the critical frequency of synchrotron emission is $\gamma^2\nu_B$. In the low-harmonic emission scenario, we are therefore considering $\gamma \gtrsim 1$ charges. Let us take $\gamma \approx 1.5$ as an estimate and postulate that the 144 MHz emission is at the second harmonic of the ambient cyclotron frequency. The kinetic temperature of the emitting electrons is then $\approx 10^{9.5}$ K, which is the limiting brightness temperature value for incoherent emission. This immediately forces a source size of 10–50 times the stellar radius. Second, harmonic emission additionally forces a magnetic field at the emitter of about 30 G. Such a strong field cannot be created in situ via energy available in the stellar wind, because if we equate the magnetic pressure in the interaction region to the ram pressure of the wind, we obtain a wind density of $\gtrsim 10^{10}$ cm^{-3} for a 500 km s^{-1} wind speed. The corresponding plasma frequency is $\approx$1 GHz, which will preclude escape of emission at 144 MHz. Therefore, the magnetic field must be carried over to tens of stellar radii from the stellar surface by an expanding admixture of thermal and mildly relativistic plasma. This is a model that is reminiscent of moving type-IV sources on the Sun (Dulk 1973), although on much larger scales and with greater magnetic field strengths. The persistence of the radio emission also requires the type-IV-like phenomena to be ever-present.

3.2. Plasma Emission

Fundamental plasma emission can be highly circularly polarized but the emergent radiation can also be depolarized due to propagation effects (Benz 1993). We therefore focus our attention on explaining the relatively flat spectrum between 144 MHz and 5 GHz that is demanded by the adherence to the Güdel–Benz relationship.

For a given level of Langmuir wave turbulence, the brightness temperature of the emergent radiation at the plasma frequency, ignoring induced emission (i.e., spontaneous emission only), is expected to be $T_b \propto \nu_p h_p$, where ν_p is the plasma frequency, and h_p is the density scale height (Zaitsev & Stepanov 1983; Stepanov et al. 2001; Vedantham 2021). Attaining a flat flux-density spectrum in the Rayleigh–Jeans regime, on the other hand, requires $T_b \propto (l\nu)^{-2}$, where l is the transverse length scale of the emitting region. These can be reconciled if $h_p l \propto \nu^{-3}$.

It is important to note here that in the stars where broad centimeter-wave observations are available, the emission extends up to at least 15 GHz (García-Sánchez et al. 2003). Ensuring a continuous plasma emission spectrum from 144 MHz to 15 GHz requires coronal density variations over 4 orders of magnitude, and the spatial distribution of density variations must follow $h_p(\nu)l(\nu) \propto \nu^{-3}$ or equivalently $h_p(n)l(n) \propto n^{-1.5}$, where n is the density. We are not aware of any physical coronal model that naturally yields these properties.

Another issue with plasma emission is the seeming absence of nonlinear effects in the centimeter-wave band. The implied radio brightness temperature at 144 MHz requires very high levels of turbulent energy approaching a fraction $w \sim 10^{-5}$ of the background plasma energy density. Such levels of turbulence are expected to lead to induced emission in the centimeter-wave band (Stepanov et al. 2001), which will lead to flux densities that are orders of magnitude larger than what is observed at 5 GHz.

For the above reasons, we find the plasma emission to be an unlikely cause of the observed radio emission.

3.3. Cyclotron Maser Instability

The cyclotron maser instability has a very high growth rate. An individual maser site can saturate on millisecond-timescales releasing a fraction of the particle energy (Melrose & Dulk 1982). Such saturation can, in principle, be used to construe a scaling between the radio and X-ray luminosities. As for the radio spectrum, a cyclotron maser is empirically known to generate somewhat flat spectra. For example, Jovian cyclotron maser emission has a flux density that stays within a factor of order unity between $\sim$1 MHz and $\approx$40 MHz (Zarka 1998). The drawback of the cyclotron maser interpretation, however, is that in RS Cvns that have been observed out

[13] Emission at low harmonics from highly relativistic charges is very inefficient.

[14] Although, in the small-pitch-angle case, the inverse Compton losses are significantly lowered compared to synchrotron losses (Woltjer 1966).

to 15 GHz, all show a continuum spectrum that is rather flat (García-Sánchez et al. 2003). A cyclotron frequency of 15 GHz implies a field strength of 5.35 kG, which has not yet been observed in Zeeman splitting detections of such stars (Donati et al. 1992; Järvinen et al. 2018; Hahlin et al. 2021).

3.4. Two Mechanisms

It could also be that the 5–15 GHz emission and the 144 MHz emission are due to two different emission mechanisms. If so, then it is remarkable that their spectral luminosities are the same. To appreciate this, consider a mildly relativistic charge that traverses the magnetic trap of length L over a timescale L/c. Cyclotron maser radiation is thought to liberate about 1% of the particle kinetic energy, which means that the energy loss rate due to cyclotron maser radiation for the charge is on average about $0.01\gamma m_e c^2/(L/c) \approx 10^{-8.5}\gamma$ erg s^{-1}. The loss rate due to synchrotron emission on the other hand is $\approx 10^{-15}\gamma^2 B^2$ erg s^{-1}, where B is in Gauss. Assuming that cyclotron maser radiation is beamed into a solid angle of about 1 sr, and taking the radio luminosity to be νL_ν, we find that flux density parity between 5 GHz and 144 MHz requires $\gamma B^2 \approx 10^9$. However, for the centimeter-wave synchrotron emission to appear at a frequency of 5 GHz requires $\gamma^2 B \approx 1800$. These two conditions cannot be simultaneously true for reasonable values of γ and B. We therefore conclude that the same charges cannot provide flux-density parity between the 144 MHz and 5 GHz emission in this scenario because cyclotron maser instability is simply too efficient.

Next consider the remaining hypothesis: the centimeter-wave emission is gyrosynchrotron in origin but the meter-wave emission is due to the plasma mechanism originally powered by the beam instability initiated by the relativistic charges that eventually emit gyrosynchrotron radiation. This scenario is significantly complicated because the plasma emission mechanism is a two-step process. In the first step, an electron beam generates Langmuir wave turbulence, and in the second step, the Langmuir waves undergo nonlinear scattering to produce transverse electromagnetic waves. The bulk of the Langmuir wave energy is likely thermalized due to nonlinear instabilities (e.g., modulational instabilities). Therefore making a feasibility argument based on energetics by appealing to first principles is rather difficult, and we do not attempt it here. We can however state that, based on the analyses of Toet et al. (2021) and Vedantham (2021), this hypothesis requires the Langmuir-wave turbulence to approach the strong turbulence limit ($w \sim 10^{-5}$) and for the 144 MHz emission region to be several stellar radii in size.

4. Summary and Outlook

Long-standing wisdom in the field of stellar radio astronomy states that highly polarized emission is coherent in nature and therefore must not follow the Güdel–Benz relationship. However, here we have demonstrated that the highly circularly polarized 144 MHz emission from active coronae unexpectedly follows the Güdel–Benz relationship, which was established using the 5 GHz (presumed) incoherent gyrosynchrotron emission. Our results, therefore, prompt a return to the drawing board to reexamine the physics behind the Güdel–Benz relationship and the thus-far presumed mechanism of radio emission from stellar coronae. We have taken the first steps in doing so here. We find that, if the 144 MHz and 5 GHz emission are assumed to be from the same mechanism, then incoherent synchrotron emission from electrons with high pitch-angle anisotropy and incoherent gyroresonance (low-harmonic synchrotron) emission from expanding plasma blobs are the most fruitful avenue to explore, whereas coherent plasma emission and cyclotron maser instability are somewhat less attractive. The incoherent mechanisms are also attractive because coherent emission is inherently highly variable, whereas our sample shows a small scatter around the Güdel–Benz relationship. We find the expanding plasma blobs model to be particularly attractive as it is phenomenologically similar to moving type-IV emission from the Sun (Dulk 1973).

If on the other hand the emission in the two radio bands is due to different mechanisms, then it is remarkable that coronal parameters in our population must conspire to yield a flux-density parity between the two radio bands. In this case, we show that the observed emission cannot be due to cyclotron maser emission at 144 MHz and gyrosynchrotron emission at 5 GHz from the same population of charges. The case of plasma emission at 144 MHz is difficult to readily constrain with available data due to the inherent two-step complexity of the plasma emission mechanism.

We end by noting that quasi-contemporaneous radio observations in the intermediate frequency range (≈200 MHz to ≈5 GHz) are now needed to address the dilemma created by our unusual results. For instance, if the 144 MHz and 5 GHz radio emissions originate from different mechanisms, then we expect to see two components in the broadband radio spectrum and/or its polarization properties. Alternatively, if emission in both radio bands is due to the gyrosynchrotron and/or gyroresonance mechanism, then we expect a relatively flat spectrum with a predictable smooth change in the polarization properties across frequency.

We thank Prof. Manuel Güdel for sharing his published data on radio and X-ray flux densities. We thank Prof. Zarka for commenting on the manuscript. H.K.V. thanks Prof. Sterl Phinney for discussions. J.R.C. thanks the Nederlandse Organisatie voor Wetenschappelijk Onderzoek (NWO) for support via the Talent Programme Veni grant. M.H. acknowledges the MSHE for granting funds for the Polish contribution to the International LOFAR Telescope (MSHE decision no. DIR/WK/2016/2017/05-1) and for maintenance of the LOFAR PL-612 Baldy (MSHE decision no. 59/E-383/SPUB/SP/2019.1) and the Polish National Agency for Academic Exchange (NAWA) within the Bekker program under grant No. PPN/BEK/2019/1/00431. T.P.R. acknowledges support from the ERC under grant No. 743029 (EASY). A.D. acknowledges support by the BMBF Verbundforschung under the grant 05A20STA. This paper is based on data obtained with the International LOFAR Telescope as part of the LoTSS survey. LOFAR is the Low-frequency Array designed and constructed by ASTRON. It has observing, data processing, and data storage facilities in several countries that are owned by various parties (each with their own funding sources) and that are collectively operated by the ILT foundation under a joint scientific policy. The ILT resources have benefited from the following recent major funding sources: CNRS-INSU, Observatoire de Paris and Université d'Orléans, France; BMBF, MIWF-NRW, MPG, Germany; Science Foundation Ireland (SFI), Department of Business, Enterprise and Innovation (DBEI), Ireland; NWO, The Netherlands; The Science and Technology Facilities Council, UK. This research made use of the Dutch national e-infrastructure with the support of the SURF Cooperative (e-infra 180169) and the LOFAR e-infra

group. The Jülich LOFAR Long Term Archive and the German LOFAR network are both coordinated and operated by the Jülich Supercomputing Centre (JSC), and computing resources on the supercomputer JUWELS at JSC were provided by the Gauss Centre for Supercomputing e.V. (grant CHTB00) through the John von Neumann Institute for Computing (NIC). This research made use of the University of Hertfordshire high-performance computing facility and the LOFAR-UK computing facility located at the University of Hertfordshire and supported by STFC [ST/P000096/1], and of the Italian LOFAR IT computing infrastructure supported and operated by INAF and by the Physics Department of Turin University (under an agreement with Consorzio Interuniversitario per la Fisica Spaziale) at the C3S Supercomputing Centre, Italy.

Software: `python3`, `numpy`, `scipy`, `matplotlib`, Telescopes: LOFAR, Services: Vizier, NASA's Astrophysics Data System.

ORCID iDs

H. K. Vedantham https://orcid.org/0000-0002-0872-181X
J. R. Callingham https://orcid.org/0000-0002-7167-1819
T. W. Shimwell https://orcid.org/0000-0001-5648-9069
A. O. Benz https://orcid.org/0000-0001-9777-9177
M. Hajduk https://orcid.org/0000-0001-6028-9932
T. P. Ray https://orcid.org/0000-0002-2110-1068
A. Drabent https://orcid.org/0000-0003-2792-1793

References

Airapetian, V. S., & Holman, G. D. 1998, ApJ, 501, 805
Benz, A. O. 1993, Plasma Astrophysics, Vol. 184 (Berlin: Springer)
Benz, A. O., & Güdel, M. 1994, A&A, 285, 621
Benz, A. O., & Güdel, M. 2010, ARA&A, 48, 241
Berger, E. 2002, ApJ, 572, 503
Berger, E., Ball, S., Becker, K. M., et al. 2001, Natur, 410, 338
Berger, E., Basri, G., Fleming, T. A., et al. 2010, ApJ, 709, 332
Boller, T., Freyberg, M. J., Trümper, J., et al. 2016, A&A, 588, A103
Callingham, J. R., Pope, B. J. S., Feinstein, A. D., et al. 2021a, A&A, 648, A13
Callingham, J. R., Vedantham, H. K., Shimwell, T. W., et al. 2021b, NatAs, 5, 1233
Davis, I., Vedantham, H. K., Callingham, J. R., et al. 2021, A&A, 650, L20
Donati, J.-F., Semel, M., & Rees, D. E. 1992, A&A, 265, 669
Drake, S. A., Simon, T., & Linsky, J. L. 1989, ApJS, 71, 905
Dulk, G. A. 1973, SoPh, 32, 491
Eker, Z., Ak, N. F., Bilir, S., et al. 2008, MNRAS, 389, 1722
Epstein, R. I. 1973, ApJ, 183, 593
Fleming, T. A., Schmitt, J. H. M. M., & Giampapa, M. S. 1995, ApJ, 450, 401
Forbrich, J., Wolk, S. J., Güdel, M., et al. 2011, in ASP Conf. Ser. 448, 16th Cambridge Workshop on Cool Stars, Stellar Systems, and the Sun, ed. C. M. Johns-Krull, M. K. Browning, & A. A. West (San Francisco, CA: ASP), 455
Gaia Collaboration, Brown, A. G. A., Vallenari, A., et al. 2018, A&A, 616, A1
García-Sánchez, J., Paredes, J. M., & Ribó, M. 2003, A&A, 403, 613
Ginzburg, V. L., & Syrovatskii, S. I. 1964, The Origin of Cosmic Rays (London: Macmillan)
Güdel, M. 2002, ARA&A, 40, 217
Güdel, M., & Benz, A. O. 1993, ApJL, 405, L63
Hahlin, A., Kochukhov, O., Alecian, E., et al. 2021, A&A, 650, A197
Hallinan, G., Antonova, A., Doyle, J. G., et al. 2008, ApJ, 684, 644
Holman, G. D. 1986, Cool Stars, Stellar Systems and the Sun (Berlin: Springer), 271
Järvinen, S. P., Hubrig, S., Scholz, R.-D., et al. 2018, MNRAS, 481, 5163
Leto, P., Trigilio, C., Krtička, J., et al. 2021, MNRAS, 507, 1979
Mandrini, C. H., Démoulin, P., & Klimchuk, J. A. 2000, ApJ, 530, 999
McLean, M., Berger, E., & Reiners, A. 2012, ApJ, 746, 23
Melrose, D. B. 1971a, ApL, 8, 35
Melrose, D. B. 1971b, Ap&SS, 12, 172
Melrose, D. B., & Dulk, G. A. 1982, ApJ, 259, 844
O'Dell, S. L., & Sartori, L. 1970, ApJL, 162, L37
Pandey, J. C., & Singh, K. P. 2012, MNRAS, 419, 1219
Rybicki, G. B., & Lightman, A. P. (ed.) 1986, Radiative Processes in Astrophysics (New York: Wiley), 400
Shimwell, T. W., Röttgering, H. J. A., Best, P. N., et al. 2017, A&A, 598, A104
Shimwell, T. W., Tasse, C., Hardcastle, M. J., et al. 2019, A&A, 622, A1
Stepanov, A. V., Kliem, B., Zaitsev, V. V., et al. 2001, A&A, 374, 1072
Tasse, C., Shimwell, T., Hardcastle, M. J., et al. 2021, A&A, 648, A1
Toet, S. E. B., Vedantham, H. K., Callingham, J. R., et al. 2021, A&A, 654, A21
van Leeuwen, F. 2007, A&A, 474, 653
Vedantham, H. K. 2021, MNRAS, 500, 3898
Vedantham, H. K., Callingham, J. R., Shimwell, T. W., et al. 2020a, ApJL, 903, L33
Vedantham, H. K., Callingham, J. R., Shimwell, T. W., et al. 2020b, NatAs, 4, 577
Vedantham, H. K., & Koopmans, L. V. E. 2016, MNRAS, 458, 3099
Williams, P. K. G., Cook, B. A., & Berger, E. 2014, ApJ, 785, 9
Woltjer, L. 1966, ApJ, 146, 597
Zaitsev, V. V., & Stepanov, A. V. 1983, SoPh, 88, 297
Zarka, P. 1998, JGR, 103, 20159